


## Stability of spin-gapless semiconducting behavior in $\text{Ti}_2\text{CoSi}$ , $\text{Ti}_2\text{MnAl}$ , and $\text{Ti}_2\text{VAs}$ Heusler compounds

Kemal Özdoğan <sup>\*</sup>*Department of Physics, Yildiz Technical University, 34210 İstanbul, Turkey*Iosif Galanakis <sup>†</sup>*Department of Materials Science, School of Natural Sciences, University of Patras, GR-26504 Patras, Greece*

 (Received 23 October 2020; revised 13 January 2021; accepted 2 February 2021; published 16 February 2021; corrected 23 February 2021)

$\text{Ti}_2\text{CoSi}$ ,  $\text{Ti}_2\text{MnAl}$ , and  $\text{Ti}_2\text{VAs}$  Heusler compounds have been identified as spin-gapless semiconductors when grown in the inverse XA lattice structure of the full-Heusler compounds. Especially  $\text{Ti}_2\text{MnAl}$  and  $\text{Ti}_2\text{VAs}$  combine this unique property with a zero magnetization being also fully compensated ferrimagnets. All three compounds are usual metals in the ground-state cubic  $L2_1$  lattice structure of the Heusler compounds. We present extensive first-principles electronic band structure calculations keeping the unit cell volume constant and varying the  $c/a$  ratio and thus both the in-plane and out-of-plane lattice parameters. Our results suggest that while  $\text{Ti}_2\text{MnAl}$  keeps its cubic character, this is not the case for  $\text{Ti}_2\text{CoSi}$  and  $\text{Ti}_2\text{VAs}$  which prefer to crystallize in tetragonal  $L2_1$ -like lattice structures with sizable  $c/a$  ratios. In this tetragonal structure both compounds are usual nonmagnetic metals losing their unique properties. Our results suggest that the stability of the cubic structure should be confirmed for all novel Heusler compounds under study and should not be considered as given. The exact behavior of each compound is materials specific and cannot be easily predicted.

DOI: [10.1103/PhysRevMaterials.5.024409](https://doi.org/10.1103/PhysRevMaterials.5.024409)

### I. INTRODUCTION

Heusler, a German metallurgist, was the first to synthesize a ternary compound,  $\text{Cu}_2\text{MnAl}$ , crystallizing in the  $L2_1$  cubic lattice structure in the beginning of the 20th Century [1,2]. Since then, hundreds of ternary and quaternary compounds crystallizing in similar cubic structures have been grown, and this family of materials has been named as Heusler compounds or Heusler alloys [3–5]. Over the past 20 years the field of magnetism has been marked by the emergence of the subfield of spintronics [6–8]. Simultaneously a new class of materials has emerged, the so-called half-metals [9]. de Groot and collaborators were the first to identify that a so-called semi-Heusler compound,  $\text{NiMnSb}$ , poses a unique electronic band structure being metallic for the majority-spin electrons and semiconducting for the minority-spin electrons [10]. The half-metallic property was later connected to the total spin magnetic moment in the case of Heusler compounds; this behavior was named as Slater-Pauling behavior [11,12]. Eventually it was found that half-metallicity was not a rare property among Heusler compounds but several of them possessed it [13]. This led to several studies where hundreds of Heusler compounds were scanned for their stability [14,15]. Hirohata and Takanashi in 2014 suggested that half-metallic Heusler compounds could have a lot of advantages for spintronic devices [16] triggering even further extended studies in this class of materials [17–21].

An even more exotic property than half-metallicity is the so-called spin-gapless semiconducting (SGS) behavior. It was initially observed in doped  $\text{PbPdO}_2$  thin films [22,23]. In these materials the one spin electronic band-structure presents a usual semiconducting behavior while the other presents a gapless semiconducting behavior (a semiconductor with a zero gap). Depending on the shape of the bands there are also several types of SGS materials (see Figs. 1 and 2 in Ref. [24]). The SGS behavior has been also predicted theoretically for several Heusler compounds: full-Heuslers crystallizing in the inverse XA lattice structure [25–27], Heusler alloys crystallizing in the  $D0_3$  lattice structure [28], and finally quaternary Heusler compounds crystallizing in the so called Y-structure [29–31]. The interest on SGS materials stems from their potential applications in spintronic devices like reconfigurable magnetic diodes and transistors suggested in Refs. [32–34] or magnetic tunnel junctions realized in Ref. [35]. Experimentally, the SGS behavior has been confirmed in the case of  $\text{Mn}_2\text{CoAl}$  an inverse full-Heusler compound [36] and in the case of the quaternary  $\text{CoFeMnSi}$  Heusler compound [37–40]. A nice review on SGS materials is provided in Ref. [24].

Among the possible SGS materials  $\text{Mn}_2\text{CoAl}$  has attracted most of the attention. Following the pioneering study of Ouardi and collaborators where they have successfully grown polycrystalline films of  $\text{Mn}_2\text{CoAl}$  and confirmed its SGS behavior [36], several other research groups have grown samples of  $\text{Mn}_2\text{CoAl}$  in various shapes and have studied them experimentally [41–50]. Electronic band structure calculations have covered a wide range of the properties of this compound like spin-waves and the temperature dependent magnetic properties [51], the role of electronic correlations [52], the stability

<sup>\*</sup>kozdogan@yildiz.edu.tr<sup>†</sup>galanakis@upatras.gr

of the SGS character [53], the heterostructures with GaAs [54], and the effect of doping [55].

## II. MOTIVATION

Except  $\text{Mn}_2\text{CoAl}$  it was suggested in Ref. [25] that also the inverse Heusler compounds based on Ti ( $\text{Ti}_2\text{MnAl}$ ,  $\text{Ti}_2\text{CoSi}$ , and  $\text{Ti}_2\text{VAs}$ ) should present SGS behavior. Even more interesting is the fact that while  $\text{Ti}_2\text{CoSi}$  is a ferromagnetic SGS with a total spin magnetic moment per formula unit (f.u.) of  $3 \mu_B$ , the other two compounds are fully compensated ferrimagnetic SGS materials with a zero total spin magnetic moment. The inverse also known as XA lattice structure occurs in the case of full-Heusler compounds when the valence of the X atom in  $\text{X}_2\text{YZ}$  chemical formula is smaller than the valence of Y and in this case the sequence of the atoms is different than in the usual full-Heusler compounds crystallizing in the  $\text{L}_{21}$  lattice structure [26]. The prediction for the choice between the  $\text{L}_{21}$  and XA lattice structures is usually referred to in literature as the empirical site preference rule [56] or the empirical lightest atom rule [18]; both rules are equivalent and result in the same predicted lattice structure. In Ref. [51] it was shown employing Monte-Carlo simulations that these three compounds have quite high Curie temperatures of 550 K ( $\text{Ti}_2\text{CoSi}$ ), 960 K ( $\text{Ti}_2\text{MnAl}$ ), and 800 K ( $\text{Ti}_2\text{VAs}$ ). Although away from the 0 K, the SGS behavior is likely to be lost, it was shown that atoms in all three compounds carry sizable atomic magnetic moments [51]. Finally in Ref. [52] it was shown employing the GW approximation that the on-site electronic correlations are not so crucial for these compounds and they keep their SGS character.

Following the prediction of the three Ti-based SGS Heusler compounds several theoretical and experimental studies have followed, confirming the results in Ref. [25] on the SGS character of these materials [57–60]. Experimentally Fend *et al.* synthesized films of  $\text{Ti}_2\text{MnAl}$  but the samples were of very low crystallinity and no safe conclusions can be drawn [54,61]. Goraus and Czerniewsky have also grown polycrystalline films of  $\text{Ti}_2\text{MnAl}$  and found that they were nonmagnetic [62]. Also in literature, several *ab initio* studies have appeared on other Ti-based Heusler compounds but none of them was found to exhibit a SGS behavior [63–69]. In 2017 Wang and collaborators published an extended study on 72 Ti-based Heusler compounds and have shown that most of them crystallize not in the inverse XA as expected but in the  $\text{L}_{21}$  lattice structure [56]. Charge density plots revealed that the mechanism behind this behavior was the strengthening of the chemical bonds [56]. Among them were also the three Ti-based compounds discussed above. It was found that  $\text{Ti}_2\text{MnAl}$  and  $\text{Ti}_2\text{VAs}$  are nonmagnetic in the  $\text{L}_{21}$  lattice structure while  $\text{Ti}_2\text{CoSi}$  is a normal ferromagnet [56]. This finding is in accordance with the nonmagnetic character of  $\text{Ti}_2\text{MnAl}$  found experimentally in Ref. [62]. A similar situation was revealed also for the Hf- and Sc-based compounds where most of them preferred the  $\text{L}_{21}$  than the XA structure which was expected to be the ground state [70,71]. But all these studies assume that the studied compounds crystallize in a cubic structure and only the sequence of the atoms in the unit cell is altered. This assumption is not justified since the tetragonal structure is well known to occur in the Mn-based

Heusler compounds [19] and there are compounds where the deformation of the lattice is so large that the  $c/a$  ratio reaches values of around 2 [72]. Fallev and collaborators have attributed the tetragonal deformation to the shape of the density of states (DOS) [19] and Wollmann and collaborators have shown that, when tetragonal deformation occurs, it leads to a strengthening of the exchange interactions and to larger values of the Curie temperature with respect to the perfect cubic lattices [72].

In 2018, Fan *et al.* and Yang *et al.* have studied the effect of uniform strain (also referred to as hydrostatic-pressure-effect in literature) and tetragonalization on the SGS properties of  $\text{Ti}_2\text{MnAl}$  [73] and  $\text{Ti}_2\text{CoSi}$  [74], respectively. In both studies the compounds have been assumed to crystallize in the inverse XA structure and not the ground-state  $\text{L}_{21}$  structure [56]. Fan *et al.* varied the  $c/a$  ratio between 0.90 and 1.10 keeping the unit cell volume constant and taking into consideration three cases: the equilibrium unit cell volume  $V_{\text{eq}}$  and the  $1.05V_{\text{eq}}$  and  $0.95V_{\text{eq}}$  cases [73]. They have shown that in all three cases the cubic  $c/a = 1$  is the energetically favorable one [73]. For  $\text{Ti}_2\text{CoSi}$ , Yang *et al.* kept the unit cell volume constant and equal to the equilibrium one and found that a  $\pm 0.2\%$  deformation destroys the SGS character of  $\text{Ti}_2\text{CoSi}$  which is now a half-metal, and a large deformation of  $-2.6\%$  or  $+4.1\%$  destroys even the half-metallic character of  $\text{Ti}_2\text{CoSi}$  [74]. Yang *et al.* have not studied the variation of the total energy with respect to the tetragonal deformation of the lattice.

Motivated by the restrictions for the cubic lattice in all previous studies on the Ti-based Heusler compounds as well as from the limited data on the effect of tetragonalization in Refs [73,74], in the present study we carry out extensive first-principles electronic band structure calculations and we show that the assumption of the cubic lattice structure is not justified. The ground state of  $\text{Ti}_2\text{CoSi}$  and  $\text{Ti}_2\text{VAs}$  is found to be tetragonal and with a particularly high  $c/a$  ratio following the sequence of the atoms in the  $\text{L}_{21}$  lattice structure.  $\text{Ti}_2\text{MnAl}$  is the only compound whose lattice was found to remain cubic being the  $\text{L}_{21}$  as suggested in Ref. [56].

## III. OUTLINE OF THE CALCULATIONS

Our study was carried out employing the full-potential nonorthogonal local-orbital minimum-basis band structure scheme (FPLO) to perform the first-principles electronic band structure calculations [75]. As exchange-correlation potential, we have used the generalized gradient approximation (GGA) as parametrized by Perdew-Burke-Ernzerhof [76], which is known to produce accurate results in the case of magnetic Heusler compounds with respect to experiments [11,12]. For all calculations the total energy (in Hartree) has been converged to the 10th decimal point and a dense  $20 \times 20 \times 20$   $\mathbf{k}$ -points grid obeying the Monkhorst-Pack scheme has been used for the integrals in reciprocal space [77].

Full-Heusler compounds of the  $\text{X}_2\text{YZ}$  chemical type, where X and Y are transition metal atoms and Z is a metalloid, usually crystallize in two possible cubic lattice structures: the regular  $\text{L}_{21}$  and the inverse XA having as prototype compounds the  $\text{Cu}_2\text{MnAl}$  and  $\text{CuHg}_2\text{Ti}$ , respectively. The former occurs always when the valence of X is larger than the valence of Y, while the latter occurs usually when the valence of X

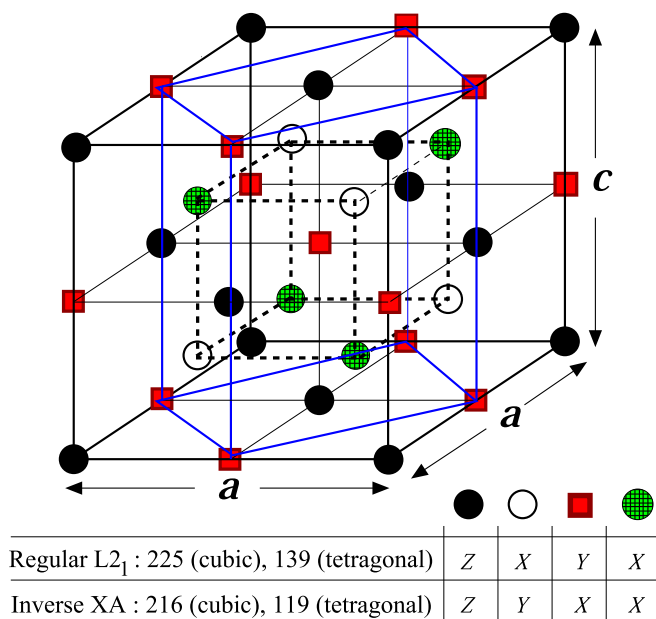


FIG. 1. Schematic representation of the two possible cubic structures of the  $X_2YZ$  Heusler compounds as well as the two structures derived when the lattice becomes tetragonal (denoted with the blue line). For each case we provide the space groups for both the cubic and tetragonal lattices.

is smaller than the valence of Y. In Fig. 1 we schematically represent both structures. The conventional unit cell is a cube ( $c/a = 1$ ) containing four primitive cells. The primitive cell, which coincides with the unit cell, is face-centered cubic like with four atoms as basis along the larger diagonal of the cube. There are four sites with Wyckoff coordinates shown in Table I. In the case of the L2<sub>1</sub> lattice structure the two X atoms occupy the B and D sites also known as 8c sites since they obey the octahedral symmetry and form a simple cubic lattice themselves. The Z and Y atoms occupy the A and C sites, respectively, known also as 4a and 4b sites since they obey the tetrahedral symmetry and they are at the center of the cubes created by the two 8c sites occupied by the X atoms. In the case of the inverse XA lattice symmetry the B and D sites obey now the tetrahedral symmetry and the 8c sites break in two inequivalent 4c and 4d sites. The sequence of the atoms along the diagonal changes now and the X atoms occupy the C and D sites while the Y atoms occupy the B sites and the Z

atoms the A sites. In Fig. 1 we present also the space group notations used for the different cases: 225 and 216 are used to denote the L2<sub>1</sub> and XA cubic structures, respectively.

When one changes the  $c/a$  ratio, then the lattices become tetragonal and the new space groups as shown in Fig. 1 are the 139 and 119, respectively, instead of the initial 225 and 216 which correspond to the L2<sub>1</sub> and XA lattice structures, respectively. One can now consider as conventional cell a rectangular parallelepiped (denoted with blue lines in Fig. 1) which contains two primitive (or unit) cells. This tetragonal cell now has the same out-of-plane  $c$  lattice parameter as the initial cubic cell but its in-plane lattice parameter,  $a_{\text{tetragonal}}$ , is the one of the cube,  $a_{\text{cubic}}$ , divided by  $\sqrt{2}$ . To make the notation more readable along the article we denote from now on as  $a$  and  $c$  the lattice parameters corresponding to the initial cubic lattices:

$$c = c_{\text{cubic}} = c_{\text{tetragonal}}, \quad (1)$$

$$a = a_{\text{cubic}} = \sqrt{2} * a_{\text{tetragonal}}. \quad (2)$$

In the case of the tetragonal lattice structures ( $c/a \neq 1$ ) the primitive cell is a bct one with four atoms again as basis and in Table I we also present the Wyckoff coordinates of these atoms.

To perform the calculations presented below, we have started from a perfect cubic lattice where both  $a$  and  $c$  lattice parameters were equal. Then we kept the volume,  $V$ , constant and varied the  $c/a$  ratio. We have performed for each one of the three  $Ti_2CoSi$ ,  $Ti_2MnAl$  and  $Ti_2VAs$  compounds such calculations for both regular and inverse lattice structures and for several initial cubes to determine accurately the ground state for each material. Although the notations L2<sub>1</sub> and XA refer to the cubic structure of the Heusler compounds, we have kept the same notation also for the tetragonal structures which have different space groups (see Fig. 1), as also done in Ref. [72], to make the sequence of the atoms in the two tetragonal structures clear to the reader.

## IV. RESULTS AND DISCUSSION

### A. The case of $Ti_2CoSi$

We will start our discussion from the  $Ti_2CoSi$  compound. In Fig. 2 we have gathered the calculated total energy as a function of the  $c/a$  ratio both for the regular L2<sub>1</sub> as well as the inverse XA lattice structures. Each line corresponds to

TABLE I. Atomic and crystal parameters of  $X_2YZ$  for cubic and tetragonal lattice structures of the studied Heusler compounds depicted in Fig. 1. For an explanation of the symbols please refer to the discussion in Sec. III.

	Cubic			Tetragonal		
	X	Y	Z	X	Y	Z
Regular	8c	4b	4a	4d	2b	2a
L2 <sub>1</sub>	$(\frac{1}{4}, \frac{1}{4}, \frac{1}{4})$ & $(\frac{3}{4}, \frac{3}{4}, \frac{3}{4})$	$(\frac{1}{2}, \frac{1}{2}, \frac{1}{2})$	(0, 0, 0)	$(0, \frac{1}{2}, \frac{1}{4})$ & $(0, \frac{1}{2}, \frac{3}{4})$	$(0, 0, \frac{1}{2})$	(0, 0, 0)
Inverse	4b	4c	4a	2b	2c	2a
XA	$(\frac{1}{2}, \frac{1}{2}, \frac{1}{2})$	$(\frac{1}{4}, \frac{1}{4}, \frac{1}{4})$	(0, 0, 0)	$(0, 0, \frac{1}{2})$	$(0, \frac{1}{2}, \frac{1}{4})$	(0, 0, 0)
	4d			2d		
	$(\frac{3}{4}, \frac{3}{4}, \frac{3}{4})$			$(0, \frac{1}{2}, \frac{3}{4})$		

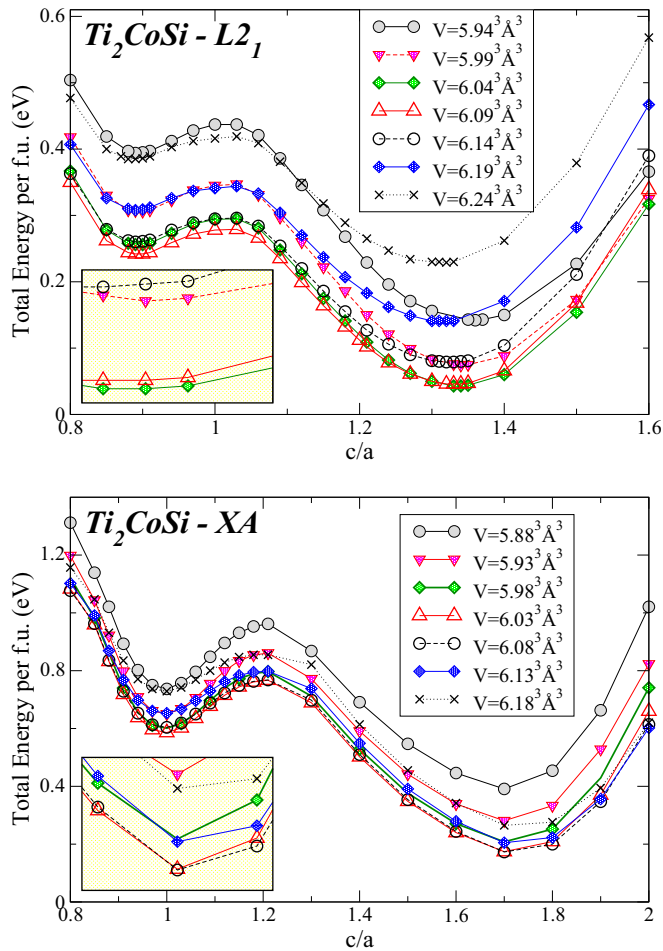


FIG. 2. Calculated total energy per formula unit (f.u.) for  $\text{Ti}_2\text{CoSi}$  and for both lattice structures regular  $L2_1$  (upper panel) and inverse XA (lower panel) as a function of the  $c/a$  ratio. Different lines correspond to different values of the volume of the conventional cell presented in Fig. 1. We have scaled the total energy in the same way for both lattice structures to get rid of the large absolute energy values. Insets present enlarged the area around the global minimum. Note that for the two panels we have used different scales for the horizontal and vertical axis.

constant volume  $V$  calculated as  $V = a^2c$ . The first observation is obvious. All lines have the same characteristics. For the  $L2_1$  lattice we get a local maximum close to the cubic case ( $c/a = 1$ ), a local minimum close to the  $c/a = 0.9$  value and a global minimum close to the  $c/a = 1.3$  value. In the case of XA again we get a local and a global minimum but now they occur for larger  $c/a$  values (note that for the two panels we have used different windows for both the horizontal and vertical axis). Now the local minimum is close to the cubic case ( $c/a = 1$ ), the local maximum is close to a  $c/a$  value of 1.2 and the global minimum is around  $c/a = 1.7$ . In the case of the XA lattice structure the gradient of the lines is larger also since they scan an energy window of 1.2 eV contrary to the case of the  $L2_1$  lattice structure where they scan an energy window of just 0.5 eV. Thus,  $L2_1$  and XA correspond to similar behaviors but not identical  $c/a$  values where the minima/maximum occur. An alternative way to present the

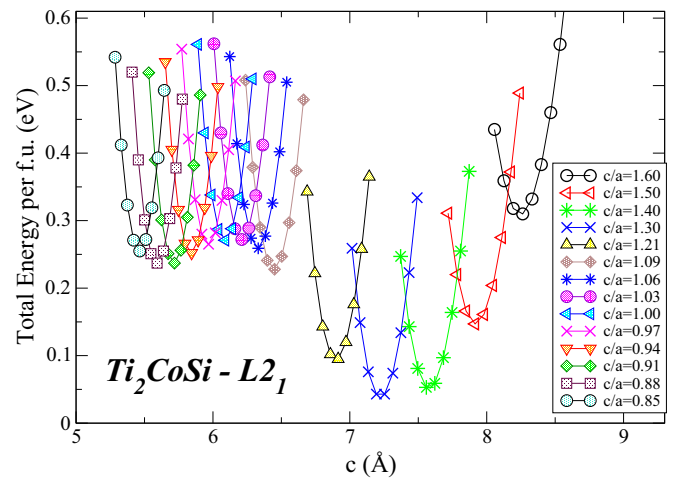


FIG. 3. We present the same information as in the upper panel of Fig. 2 for the  $L2_1$  lattice structure of  $\text{Ti}_2\text{CoSi}$ . Now we keep the  $c/a$  constant and plot the total energy per f.u. as a function of the  $c$  out-of-plane lattice parameter (see Fig. 1 for the structure).

results in Fig. 2 is to plot the calculated total energy values as a function of the  $c$  lattice parameter. This is shown in Fig. 3 for the  $L2_1$  case. As shown for a constant  $c/a$  value the total energy versus the  $c$  lattice constant shows a parabolic behavior. From all calculated lines the one corresponding to  $c/a = 1.30$  shows the global minimum among all calculated values. This value is close to the 1.34 corresponding to the ground state.

To make the vertical energy axis easier to read we have shifted the total energy with the same amount for both lattice structures. Thus, it is easy to deduce already from the graphs that the global minimum for the lowest volume line is lower in the case of the  $L2_1$  lattice structure than for the XA one. Thus, although the energy corresponds to a tetragonal and not a cubic lattice structure, the  $L2_1$  structure is the stable one, in accordance with the results of Wang *et al.* for the cubic lattices [56]. Since it is not easy to quantify the results using the graphs in Figs. 2 and 3, we have gathered in Table II the numerical data concerning all the studied cases of interest. For  $\text{Ti}_2\text{CoSi}$  and for both XA and  $L2_1$  structures we have first gathered the structural parameters at the local and global minima as well when imposing the cubic structure. In the case of the  $L2_1$  lattice the global minimum occurs for a  $c/a$  ratio of 1.34 while in the case of the XA structure for a 1.73 value and the lattice it this case shows a more pronounced tetragonalization effect. In the  $L2_1$  case the local minimum is slightly below the perfect cubic ratio while in the case of the XA lattice the local minimum is very close to the perfect  $c/a = 1$  case. Of interest are the energy differences presented in the last column. The energy difference between the global and the local minimum in the case of the  $L2_1$  lattice structure is  $-0.199$  eV while in the case of the XA lattice it is  $-0.417$  eV being much larger. Overall the global minimum in the  $L2_1$  structure is 0.126 eV lower than the in the XA case meaning that the  $L2_1$  is the ground state with  $c/a = 1.34$ ,  $a = 5.479$  Å and  $c = 7.341$  Å.

Of interest are also the magnetic properties of the studied cases and in Table II we present also the atom-resolved spin

TABLE II. For each one of the three compounds and for both structures we present the structural and magnetic properties in the case of the global minimum, the local minimum and the minimum assuming perfect cubic lattices. For  $\text{Ti}_2\text{MnAl}$  there is just one minimum at the perfect cubic lattice. In the case of the XA structure for the spin magnetic moments the first Ti atom sits at the 2b site and the second Ti atom sits at the 2d site (see Table I). Last column presents various energy differences (see text for discussion).

Compound			$c/a$	$a$ (Å)	$c$ (Å)	Spin moments ( $\mu_B$ )				Total	Energy differences
						Ti	Co/Mn/V	Ti	Si/Al/As		
$\text{Ti}_2\text{CoSi}$	L2 <sub>1</sub>	Global min.	1.34	5.479	7.341	0.151	0.822	0.151	-0.008	1.116	$\Delta E_{L2_1}^{\text{Glob.-Local}}$
		Cubic	1	6.090	6.090	0.567	1.337	0.567	0.083	2.554	-0.199 eV
		Local min.	0.89	6.331	5.635	0.336	1.343	0.336	0.080	2.095	$\Delta E_{XA}^{\text{Glob.-Local}}$
	XA	Global min.	1.73	5.064	8.762	0.000	0.000	0.000	0.000	0.000	-0.417 eV
		Cubic	1	6.030	6.030	1.802	0.351	0.865	-0.018	3.000	$\Delta E_{\text{Global min.}}^{L2_1-XA}$
		Local min.	0.99	6.050	5.990	1.802	0.351	0.865	-0.018	3.000	-0.126 eV
$\text{Ti}_2\text{MnAl}$	L2 <sub>1</sub>	Cubic	1	6.160	6.160	0.000	0.000	0.000	0.000	0.000	$\Delta E^{L2_1-XA}$
	XA	Cubic	1	6.240	6.240	1.443	-2.738	1.303	-0.009	0.000	-0.209 eV
$\text{Ti}_2\text{VAs}$	L2 <sub>1</sub>	Global min.	1.47	5.506	8.093	-0.019	1.151	-0.019	-0.032	1.081	$\Delta E_{L2_1}^{\text{Glob.-Local}}$
		Cubic	1	6.210	6.210	0.000	0.000	0.000	0.000	0.000	-0.158 eV
		Local min.	0.98	6.252	6.127	0.000	0.000	0.000	0.000	0.000	$\Delta E_{XA}^{\text{Glob.-Local}}$
	XA	Global min.	1.60	5.370	8.591	-0.141	-1.045	-0.449	0.042	-1.593	-0.365 eV
		Cubic	1	6.230	6.230	1.305	-1.856	0.535	0.009	-0.008	$\Delta E_{\text{Global min.}}^{L2_1-XA}$
		Local min.	0.98	6.272	6.147	1.301	-1.850	0.532	0.009	-0.008	-0.001 eV

magnetic moments as well as the total spin magnetic moment per unit cell or formula unit (they coincide in our case). First for the XA structure we see that for both the cubic case as well as the local minimum case we get a total spin magnetic moment of  $3 \mu_B$  in accordance to the one predicted by the Slater-Pauling rule and similar to previous calculations [25]. If we look at the total density of states (DOS) plotted in Fig. 4, in that case we have a perfect SGS material since in the majority-spin band structure the valence and conduction bands touch each other and we have a zero gap semiconducting behavior. Interestingly the global minimum for the XA lattice corresponds to a non magnetic usual metallic state as shown both by the calculated spin magnetic moments in Table II and the calculated DOS in Fig. 4. We have repeated these calculations several times starting with various initial spin magnetic moments for the various chemical elements but we always converged to the non magnetic state. It seems that the large degree of tetragonalization, which results to small in-plane distance of the Ti atoms within the plane, kills the magnetism in this case (note that as shown in Fig. 1 the in-plane distance of two Ti-atoms in the XA structure is  $a/\sqrt{2}$ ). Contrary to the XA lattice structure in the case of the L2<sub>1</sub> lattice in all cases we get a magnetic metallic state as shown also in the upper panel of Fig. 4. The total spin magnetic moment is larger in the cubic case and as we go to the local or global minimum and tetragonalize our lattice, the total spin magnetic moment is reduced. The behavior of the atomic spin magnetic moments is not easy to be explained since as we tetragonalize the lattice we change the distance between the nearest neighboring Ti-Co atoms as well as between the next-nearest neighboring Ti-Ti atoms. This affects the hybridization effects between the  $d$  orbitals of neighboring atoms and affects the final magnetic moments of the compound.

The atom-resolved spin magnetic moments do not present some peculiarity in the magnetic cases although the same atoms carry quite different spin magnetic moments in the L2<sub>1</sub> and XA cases. In the L2<sub>1</sub> lattice structures Co atoms at the

2b sites have eight Ti atoms as nearest neighbors and they are the ones which carry the main part of the magnetic moment while the Ti atoms carry sizable although smaller magnetic moments. In the case of the XA lattice structure the situation is reversed. Now the Ti atoms at the 2b sites are at the center of a cube having four Ti atoms at the 2d and four Co atoms at the 2c sites as nearest neighbors at the corners of the cube (see Table I for the definition). Thus, in the magnetic cases, the Ti atoms at the 2b sites are the ones carrying the main part of the spin magnetic moment which is about  $1.8 \mu_B$ . The Co atoms still carry a sizable spin magnetic moment reaching  $0.9 \mu_B$  while the Ti atoms at the 2d sites carry a spin magnetic moment of about  $0.35 \mu_B$ . These results confirm the assumption usually made for Heusler compounds that the symmetry is more important than the chemical species themselves [12].

Finally, we should also shortly discuss the mechanisms between the structural behavior of  $\text{Ti}_2\text{CoSi}$ . The preference towards the L2<sub>1</sub> lattice is well grounded in Ref. [56] where it was shown in the case of several Ti-based Heusler compounds that the chemical bonds are stronger in the case of the L2<sub>1</sub> lattice structure compared to the XA lattice. However, the tetragonalization has been already observed largely in the case of the Mn-based Heusler compounds having the chemical formula  $\text{Mn}_2\text{YZ}$  where Y is a transition metal atom and Z a metalloid [72]. Faleev and collaborators argued in Ref. [19] that this is due to the shape of the DOS which plays a crucial role towards this behavior and that the tetragonalization reduces the DOS around the Fermi level leading to smaller total energy values. If we look at our calculated DOS for the XA lattice in Fig. 4 exactly at the Fermi level (zero energy in the horizontal axis), the DOS at the Fermi level is zero for the less stable cubic structure and sizable in the stable tetragonal lattice. In the case of the L2<sub>1</sub> lattice structure exactly at the Fermi level the DOS for both the cubic lattice and at the global minimum has similar values. If we look not exactly at the Fermi level but just below it in the tetragonal cases, there are less pronounced peaks in the DOS and this may lead

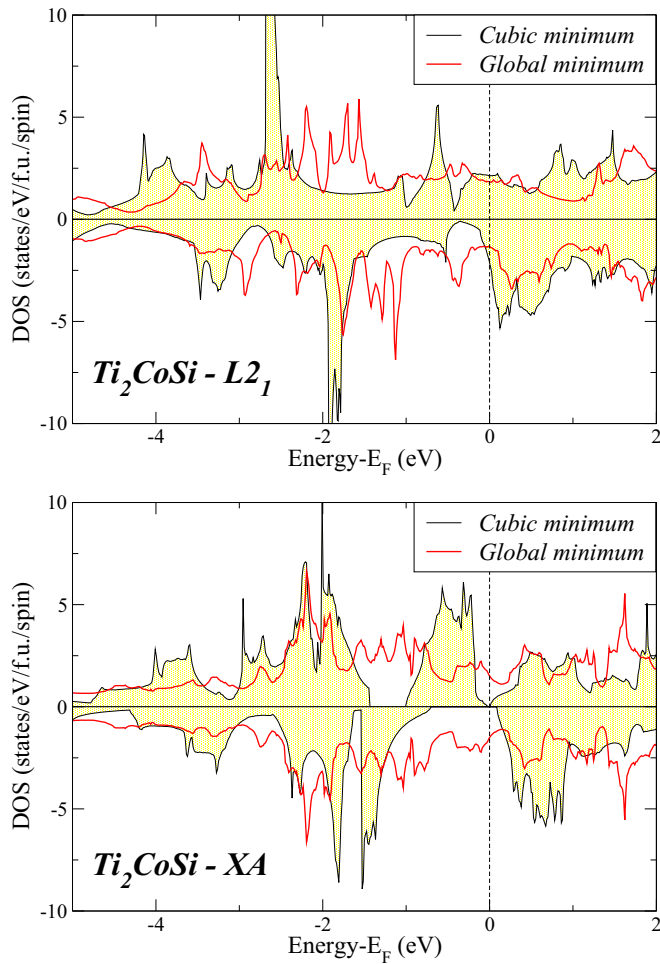


FIG. 4. Density of states (DOS) calculated in units states/eV/f.u./spin as a function of the energy for  $\text{Ti}_2\text{CoSi}$  in both  $L2_1$  (upper panel) and XA (lower panel) lattice structures. We present for each case the DOS at the global energy minimum (corresponding to the ground state) and the total energy minimum assuming a perfect cubic lattice. Positive (negative) DOS values correspond to the majority (minority)-spin electrons. The zero energy value in the horizontal axis is associated to the Fermi level.

to the stability of the tetragonal lattice compared to the cubic one.

### B. The case of the $\text{Ti}_2\text{MnAl}$ and $\text{Ti}_2\text{VAs}$ compounds

Next we will focus on the properties of the  $\text{Ti}_2\text{MnAl}$  compound.  $\text{Ti}_2\text{MnAl}$  combines the spin-gapless semiconducting behavior with a fully compensated ferrimagnetic behavior when grown in the cubic XA lattice structure [25]. Moreover in Ref. [56] this compound was shown to assume the  $L2_1$  instead of the XA lattice structure when cubic symmetry is imposed and in the  $L2_1$  ground state it was found not to be magnetic. We have repeated also for this compound similar calculations as for the  $\text{Ti}_2\text{CoSi}$  compounds where we have calculated the total energy versus the  $c/a$  ratio keeping the volume of the conventional cell constant. For the  $L2_1$  lattice we performed calculations varying the volume from  $6.01^3 \text{ \AA}^3$  up to  $6.31^3 \text{ \AA}^3$  increasing in each step the basis by  $0.05 \text{ \AA}^3$ .

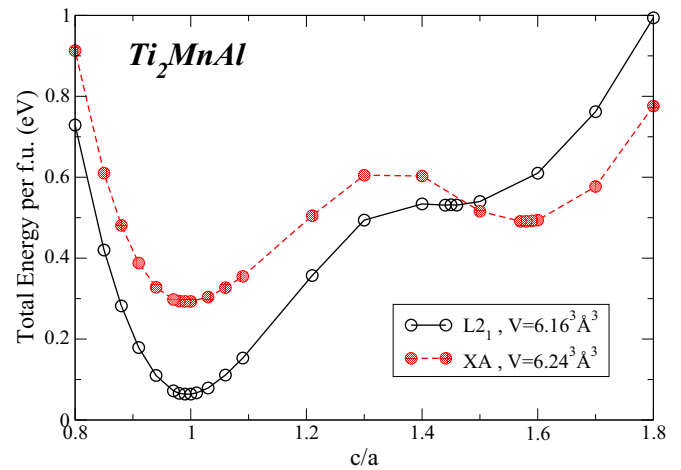


FIG. 5. Similar to Fig. 2. We present for  $\text{Ti}_2\text{MnAl}$  one constant-volume case for each lattice structure. The selected  $V$  values correspond to the global minimum for each lattice structure.

In the case of the XA structure we used the same increment for the basis and we varied the volume between  $6.09^3 \text{ \AA}^3$  and  $6.39^3 \text{ \AA}^3$ . In Fig. 5 we present one such line per lattice structure for a volume corresponding to the minimum energy. All calculated lines had exactly the same shape being almost parallel as in the case of  $\text{Ti}_2\text{CoSi}$  presented above. Now contrary to  $\text{Ti}_2\text{CoSi}$ , the global minimum for each line occurs at the cubic case ( $c/a = 1$ ) while only in the case of XA there is also a local minimum for a  $c/a$  ratio close to 1.6 which is about 0.2 eV higher than the global minimum. The ground state is the  $L2_1$  cubic lattice structure with a lattice parameter of  $6.16 \text{ \AA}$ . As shown in Table II the energy difference between the  $L2_1$  and the XA global minima is about  $-0.2 \text{ eV}$  which means that possibly  $\text{Ti}_2\text{MnAl}$  could eventually be grown in the XA structure, which shows the interesting magnetic properties, as a metastable phase in the form of a thin film. The XA structure corresponds to a fully compensated ferrimagnetic

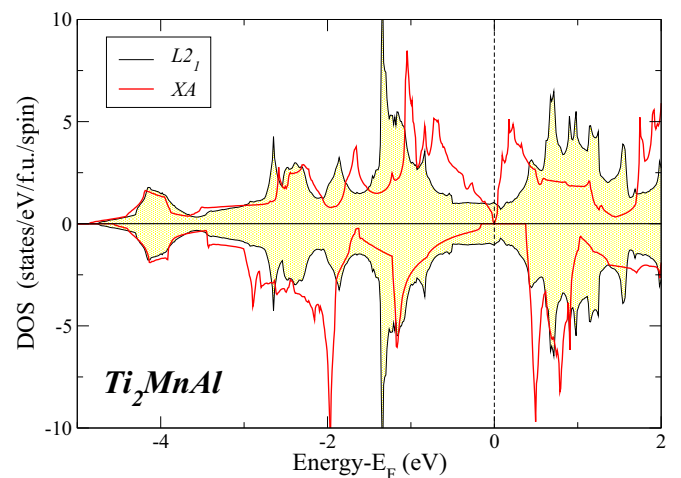


FIG. 6. DOS at the total energy minimum for the  $\text{Ti}_2\text{MnAl}$  compound and for both  $L2_1$  and XA lattice structures. Note that  $\text{Ti}_2\text{MnAl}$  retains its cubic lattice at the energy minimum for both structures. Details as in Fig. 5.

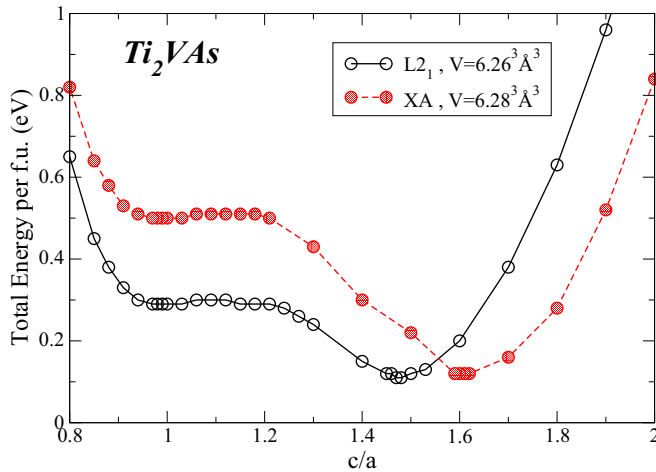


FIG. 7. Similar to Fig. 5 for the  $Ti_2VAs$  compound. We have chosen  $V$  values close to the ones which correspond to the global minimum.

state since the large spin magnetic moment at the Mn site is counterbalanced by the spin magnetic moments of the two Ti atoms as shown in Table II. Moreover in Fig. 6 we have plotted the DOS where it is obvious that in the case of the XA lattice  $Ti_2MnAl$  exhibits a spin-gapless semiconducting behavior. These results for the XA lattice structure agree with the results in Ref. [25]. In the case of the  $L2_1$  ground state the compound is not magnetic and shows metallic behavior as shown in Fig. 6. This behavior agrees with the experimental data in Ref. [62].

Finally, we shall discuss the case of the  $Ti_2VAs$  compound. In the XA structure it is well known that it also combines spin-gapless semiconducting behavior with the fully compensated ferrimagnetic one [25]. As for  $Ti_2MnAl$  we have performed calculations keeping the conventional unit cell volume constant and varying the  $c/a$  ratio. For the  $L2_1$  lattice the volume was varied from  $6.06^3 \text{ \AA}^3$  up to  $6.36^3 \text{ \AA}^3$  and for the XA lattice structure the volume was varied between  $6.08^3 \text{ \AA}^3$  and  $6.38^3 \text{ \AA}^3$  (in both cases between two consecutive sets of calculations we increased the basis in the volume by  $0.05 \text{ \AA}^3$ ). Similar to  $Ti_2MnAl$  we present in Fig. 7 the calculated total energy versus the  $c/a$  ratio for one volume close to the equilibrium and for both possible structures. Now the obtained lines are similar to the results for  $Ti_2CoSi$ . There is a pretty flat region close to the cubic case and local minima is obtained for a ratio slightly smaller than the ideal  $c/a = 1$  value. The global minimum in each case corresponds to a pretty large value of the  $c/a$  ratio: 1.47 for the  $L2_1$  lattice structure and 1.60 for the XA lattice structure. The energy difference between the local minimum and the global minimum is quite large especially for the XA lattice where it reaches a value of 0.365 eV as shown in Table II. What makes  $Ti_2VAs$  very interesting for applications is the very small difference between the two global minima for the two lattice structures.

The  $L2_1$  structure is more stable just by a tiny 0.001 eV as can be seen also in Fig. 7, and thus it is highly possible to grow the XA structure of  $Ti_2VAs$  instead of the  $L2_1$  in experiments depending on the growth/deposition conditions. Unfortunately, in the tetragonal XA lattice structure  $Ti_2VAs$  is no more a spin-gapless semiconductor and its total spin magnetic moment instead of being zero as in the cubic case reaches a value of about  $1.6 \mu_B$  and the fully compensated ferrimagnetism is destroyed. In the case of the  $L2_1$  structure the hybridization between the V  $3d$  orbitals and the  $3d$  orbitals of the eight neighboring Ti atoms is very weak and at the global minimum only V carries a sizable spin magnetic moment while at the plateau the material is a nonmagnetic metal. Notice that for all the nonmagnetic cases in Table II we have performed several calculations starting from different initial distributions of the spin magnetic moments but we always converged to the nonmagnetic state.

## V. SUMMARY AND CONCLUSIONS

Ti-based Heuslers compounds and alloys are widely studied recently both theoretically and experimentally. The interest emerges from the discovery that  $Ti_2CoSi$ ,  $Ti_2MnAl$ , and  $Ti_2VAs$  are spin-gapless semiconductors when grown in the inverse XA lattice structure of the full-Heusler compounds [25]. Moreover the latter two combine this unique property with a zero magnetization being also fully compensated ferrimagnets. Recently, it was argued that these compounds prefer actually the regular  $L2_1$  lattice structure of the Heusler compounds for which they are usual metals losing even their magnetic properties in some cases [56]. The common characteristic of all these studies is that they have assumed always that the lattice remains cubic. This assumption is not justified since the Mn-based compounds are well-known to prefer the tetragonal analog of these structures and with a very large  $c/a$  ratio [72]. Motivated by this observation we have performed extensive first-principles electronic band structure calculations keeping the unit cell volume constant and varying the  $c/a$  ratio and thus both the in-plane and out-of-plane lattice parameters. Our results suggest that while  $Ti_2MnAl$  keeps its cubic character, this is not the case for  $Ti_2CoSi$  and  $Ti_2VAs$ . The latter, both in the XA and  $L2_1$  structures, prefer to tetragonalize their lattices and with pretty large  $c/a$  ratios. The  $L2_1$  tetragonal configuration is the ground state although in the case of  $Ti_2VAs$  the energy difference between the two lattice structures is almost vanishing. But away from the cubic case, both  $Ti_2CoSi$  and  $Ti_2VAs$  lose their unique magnetic characteristics and are common metallic materials. Taking into account the structural properties of all three studied compounds, it seems that the exact behavior is materials specific and no safe general predictions can be made. We expect that our current study will trigger further interest both experimental and theoretical on this class of materials for spintronic applications.

[1] F. Heusler, *Verh. Dtsch. Phys. Ges.* **5**, 219 (1903).

[2] F. Heusler and E. Take, *Phys. Z.* **13**, 897 (1912).

[3] P. J. Webster, *Contemp. Phys.* **10**, 559 (1969).

[4] P. J. Webster and K. R. A. Ziebeck, *Alloys and Compounds of d-Elements with Main Group Elements. Part 2*, edited by H. P. J. Wijn, Landolt-Börnstein,

- New Series, Group III, Vol. 19c (Springer, Berlin, 1988) pp. 75–184.
- [5] K. R. A. Ziebeck and K.-U. Neumann, *Magnetic Properties of Metals*, edited by H. P. J. Wijn, Landolt-Börnstein, New Series, Group III, Vol. 32c (Springer, Berlin, 2001) pp. 64–414.
- [6] S. A. Wolf, D. D. Awschalom, R. A. Buhrman, J. M. Daughton, S. von Molnar, M. L. Roukes, A. Y. Chtchelkanova, and D. M. Treger, *Science* **294**, 1488 (2001).
- [7] I. Žutić, J. Fabian, and S. D. Sarma, *Rev. Mod. Phys.* **76**, 323 (2004).
- [8] C. Felser and G. H. Fecher (eds.), *Spintronics: From Materials to Devices*, 1st ed. (Springer, Netherlands, 2013).
- [9] M. I. Katsnelson, V. Y. Irkhin, L. Chioncel, A. I. Lichtenstein, and R. A. de Groot, *Rev. Mod. Phys.* **80**, 315 (2008).
- [10] R. A. de Groot, F. M. Mueller, P. G. Van Engen, and K. H. J. Buschow, *Phys. Rev. Lett.* **50**, 2024 (1983).
- [11] I. Galanakis, P. H. Dederichs, and N. Papanikolaou, *Phys. Rev. B* **66**, 134428 (2002).
- [12] I. Galanakis, P. H. Dederichs, and N. Papanikolaou, *Phys. Rev. B* **66**, 174429 (2002).
- [13] T. Graf, C. Felser, and S. S. P. Parkin, *Prog. Solid State Chem.* **39**, 1 (2011).
- [14] M. Gilleßen and R. Dronskowski, *J. Comput. Chem.* **30**, 1290 (2009).
- [15] M. Gilleßen and R. Dronskowski, *J. Comput. Chem.* **31**, 612 (2010).
- [16] A. Hirohata and K. Takanashi, *J. Phys. D: Appl. Phys.* **47**, 193001 (2014).
- [17] C. Felser and A. Hirohata, eds., *Heusler Alloys: Properties, Growth, Applications*, 1st ed., Springer Series in Materials Science, Vol. 222 (Springer International Publishing, Switzerland, 2005).
- [18] S. V. Faleev, Y. Ferrante, J. Jeong, M. G. Samant, B. Jones, and S. S. P. Parkin, *Phys. Rev. B* **95**, 045140 (2017).
- [19] S. V. Faleev, Y. Ferrante, J. Jeong, M. G. Samant, B. Jones, and S. S. P. Parkin, *Phys. Rev. Appl.* **7**, 034022 (2017).
- [20] S. V. Faleev, Y. Ferrante, J. Jeong, M. G. Samant, B. Jones, and S. S. P. Parkin, *Phys. Rev. Mater.* **1**, 024402 (2017).
- [21] J. Ma, J. He, D. Mazumdar, K. Munira, S. Keshavarz, T. Lovorn, C. Wolverton, A. W. Ghosh, and W. H. Butler, *Phys. Rev. B* **98**, 094410 (2018).
- [22] X. Wang, *Phys. Rev. Lett.* **100**, 156404 (2008).
- [23] X. Wang, G. Peleckis, C. Zhang, H. Kimura, and S. Dou, *Adv. Mater.* **21**, 2196 (2009).
- [24] Z. Yue, Z. Li, S. L., and X. Wang, *Small* **16**, 1905155 (2020).
- [25] S. Skaftouros, K. Özdoğan, E. Şaşıoğlu, and I. Galanakis, *Appl. Phys. Lett.* **102**, 022402 (2013).
- [26] S. Skaftouros, K. Özdoğan, E. Şaşıoğlu, and I. Galanakis, *Phys. Rev. B* **87**, 024420 (2013).
- [27] I. Galanakis, K. Özdoğan, and E. Şaşıoğlu, *AIP Adv.* **6**, 055606 (2016).
- [28] G. Y. Gao and K.-L. Yao, *Appl. Phys. Lett.* **103**, 232409 (2013).
- [29] K. Özdoğan, E. Şaşıoğlu, and I. Galanakis, *J. Appl. Phys.* **113**, 193903 (2013).
- [30] Q. Gao, I. Opahle, and H. Zhang, *Phys. Rev. Mater.* **3**, 024410 (2019).
- [31] G. Z. Xu, E. K. Liu, Y. Du, G. J. Li, G. D. Liu, W. H. Wang, and G. H. Wu, *Europhys. Lett.* **102**, 17007 (2013).
- [32] E. Şaşıoğlu, S. Blügel, and I. Mertig, *Appl. Electron. Mater.* **1**, 1552 (2019).
- [33] E. Şaşıoğlu, T. Aull, D. Kutschabsky, S. Blügel, and I. Mertig, *Phys. Rev. Appl.* **14**, 014082 (2020).
- [34] T. Aull, E. Şaşıoğlu, I. V. Maznichenko, S. Ostanin, A. Ernst, I. Mertig, and I. Galanakis, *Phys. Rev. Mater.* **3**, 124415 (2019).
- [35] L. Bainsla, K. Z. Suzuki, M. Tsujikawa, H. Tsuchiura, M. Shirai, and S. Mizukami, *Appl. Phys. Lett.* **112**, 052403 (2018).
- [36] S. Ouardi, G. H. Fecher, C. Felser, and J. Kübler, *Phys. Rev. Lett.* **110**, 100401 (2013).
- [37] L. Bainsla, A. I. Mallick, M. M. Raja, A. K. Nigam, B. S. D. C. S. Varaprasad, Y. K. Takahashi, A. Alam, K. G. Suresh, and K. Hono, *Phys. Rev. B* **91**, 104408 (2015).
- [38] L. Bainsla, A. I. Mallick, M. M. Raja, A. A. Coelho, A. K. Nigam, D. D. Johnson, A. Alam, and K. G. Suresh, *Phys. Rev. B* **92**, 045201 (2015).
- [39] L. Bainsla, R. Yilgin, J. Okabayashi, A. Ono, K. Suzuki, and S. Mizukami, *Phys. Rev. B* **96**, 094404 (2017).
- [40] H. E. Fu, C. Y. You, F. Q. Xin, L. Ma, and N. Tian, *Appl. Phys. Lett.* **112**, 262406 (2018).
- [41] K. Arima, F. Kuroda, S. Yamada, T. Fukushima, T. Oguchi, and K. Hamaya, *Phys. Rev. B* **97**, 054427 (2018).
- [42] K. Ueda, S. Hirose, and H. Asano, *Appl. Phys. Lett.* **110**, 202405 (2017).
- [43] P. Chen, C. Gao, G. Chen, K. Mi, P. Liu, M. abd Zhang, and D. Xue, *Appl. Phys. Lett.* **113**, 122402 (2018).
- [44] Z. Chen, W. Liu, P. Chen, X. Ruan, J. Sun, R. Liu, C. Gao, J. Du, B. Liu, H. Meng, R. Zhang, and Y. Xu, *Appl. Phys. Lett.* **117**, 012401 (2020).
- [45] N. Y. Sun, Y. Q. Zhang, H. R. Fu, W. R. Che, C. Y. You, and R. Shan, *AIP Adv.* **6**, 015006 (2016).
- [46] M. E. Jamer, B. A. Assaf, T. Devakul, and D. Heiman, *Appl. Phys. Lett.* **103**, 142403 (2013).
- [47] M. E. Jamer, B. A. Assaf, G. E. Sterbinsky, D. A. Arena, and D. Heiman, *J. Appl. Phys.* **116**, 213914 (2014).
- [48] G. Z. Xu, Y. Du, X. M. Zhang, H. G. Zhang, E. K. Liu, W. H. Wang, and W. G. H., *Appl. Phys. Lett.* **104**, 242408 (2014).
- [49] X. D. Xu, Z. X. Chen, Y. Sakuraba, A. Perumal, K. Masuda, L. S. D. Kumara, H. Tajiri, T. Nakatani, J. Wang, W. Zhou, Y. Miura, T. Ohkubo, and H. K., *Acta Mater.* **176**, 33 (2019).
- [50] R. G. Buckley, T. Butler, C. Pot, N. M. Strickland, and S. Granvill, *Mater. Res. Express* **6**, 106113 (2019).
- [51] A. Jakobsson, P. Mavropoulos, E. Şaşıoğlu, S. Blügel, M. Ležaić, B. Sanyal, and I. Galanakis, *Phys. Rev. B* **91**, 174439 (2015).
- [52] M. Tas, E. Şaşıoğlu, C. Friedrich, and I. Galanakis, *J. Magn. Magn. Mater.* **441**, 333 (2017).
- [53] I. Galanakis, K. Özdoğan, E. Şaşıoğlu, and S. Blügel, *J. Appl. Phys.* **115**, 093908 (2014).
- [54] Y. Feng, C.-L. Tian, H.-K. Yuan, A.-L. Kuang, and H. Chen, *J. Phys. D: Appl. Phys.* **48**, 445003 (2015).
- [55] R. Dhakal, S. Nepal, R. B. Ray, R. Paudel, and K. G. C., *J. Magn. Magn. Mater.* **503**, 166588 (2020).
- [56] X. Wang, Z. Cheng, H. Yuan, and R. Khenata, *J. Mat. Chem. C* **5**, 11559 (2017).
- [57] A. Birsan, P. Palade, and V. Kuncser, *J. Magn. Magn. Mater.* **331**, 109 (2013).
- [58] J. Han and G. Gao, *Appl. Phys. Lett.* **113**, 102402 (2018).
- [59] Y. J. Zhang, Z. Liu, L. G. D., X. Q. Ma, and Z. X. Cheng, *J. Magn. Magn. Mater.* **449**, 515 (2018).
- [60] L. Zhang, S. Dong, Y.-L. Du, J. abd Lu, H. Zhao, and L. Feng, *Appl. Sci.* **10**, 782 (2020).



- [61] W. Feng, X. Fu, C. Wan, Z. Yuan, X. Han, N. V. Quang, and S. Cho, *Phys. Status Solidi RRL Rapid Res. Lett* **9**, 641 (2016).
- [62] J. Goraus and J. Czerniewski, *J. Magn. Magn. Mater.* **498**, 166106 (2020).
- [63] K. H. Sadeghi and F. Ahmadian, *Pramana – J. Phys.* **90**, 16 (2018).
- [64] Y. Wen, X. Yu, X. Zeng, Y. Ye, D. Wu, and Q. Gou, *Eur. Phys. J. B* **91**, 140 (2018).
- [65] L. Hao, P. Cheng, R. Khenata, P.-F. Liu, X. Wang, and T. Yang, *J. Magn. Magn. Mater.* **505**, 166880 (2020).
- [66] L. Feng and X. Y. Zhang, *Phys. Lett. A* **383**, 243 (2019).
- [67] H. Luo, B. Liu, S. Li, Y. in, F. Meng, H. Liu, and E. Liu, *Sol. St. Commun.* **292**, 7 (2019).
- [68] J. LI, Q. Zhang, J. Li, G. Yang, H. Ma, G. Zhou, Z. Lu, W. Fang, H. Xie, C. Liang, and F. Yin, *Intermetallics* **85**, 149 (2017).
- [69] G. Taşkin, N. Atiş, O. Canko, S. Kervan, and N. Kervan, *J. Magn. Magn. Mater.* **426**, 473 (2017).
- [70] X. Wang, Z. Cheng, and W. Wang, *Materials* **10**, 1200 (2017).
- [71] Y. Han, Z. Chen, M. Kuang, Z. Liu, X. Wang, and X. Wang, *Res. Phys.* **12**, 435 (2019).
- [72] L. Wollmann, S. Chadov, J. Kübler, and C. Felser, *Phys. Rev. B* **92**, 064417 (2015).
- [73] X. Fan, J. Li, and Y. Jin, *Mod. Phys. Lett. B* **32**, 1850153 (2018).
- [74] T. Yang, L. Hao, R. Khenata, and X. Wang, *Materials* **11**, 2091 (2018).
- [75] K. Koepernik and H. Eschrig, *Phys. Rev. B* **59**, 1743 (1999).
- [76] J. P. Perdew, K. Burke, and M. Ernzerhof, *Phys. Rev. Lett.* **77**, 3865 (1996).
- [77] H. J. Monkhorst and J. D. Pack, *Phys. Rev. B* **13**, 5188 (1976).
- Correction:* The original Reference [72] contained partial misinformation that disabled proper linkage, which has been properly rendered now.